J. Shanghai Jiao Tong Univ. (Sci.), 2022
https://doi.org/10.1007/s12204-022-2552-0

Longitudinal Motion Simulation of Stratospheric Airship Under Dynamic Response of Moving-Mass Actuator

XU Minjie[1,2] (徐敏杰), *WANG Quanbao*[1*] (王全保), *DUAN Dengping*[1] (段登平)
(1. School of Aeronautics and Astronautics, Shanghai Jiao Tong University, Shanghai 200240, China;
2. Northwest Institute of Nuclear Technology, Xi'an 710024, China)

Abstract: In this paper, a design method of moving-mass stratospheric airship with constant total mass is presented, and the general dynamics equation based on Newton-Euler method is derived. Considering the time-delay of the slider command response and the dynamic coupling to the airship's state parameters, a position tracking controller with input and state constraints was designed to make the dynamic response system of the slider have critical damping characteristics. By taking the longitudinal attitude motion of moving-mass stratospheric airship as the research object, parametric modeling and attitude control simulation were carried out, and the attitude control ability of moving-mass control under different mass ratios was analyzed. The simulation results show that the attitude control ability is not affected by airspeed, and the mass ratio of slider is the main factor affecting the attitude control ability. The parameters of the slider controller have a direct influence on the dynamic performance of attitude control and also determine the dynamic coupling level of the airship. Compared with the attitude control based on the aerodynamic control surface, moving-mass control can make the airspeed and attack angle converged to the initial state at the steady state, and keep a good aerodynamic shape.
Key words: stratospheric airship, slider, dynamic response, attitude control
CLC number: V 249 **Document code:** A

0 Introduction

Stratospheric airship is a typical low-dynamic aerostat in near space[1]. It has great application prospects in the fields of earth observation, satellite-ground communication, radio relay, high-altitude scientific experiments and military application requirements due to its unique advantages such as high efficiency-cost ratio, all-weather operation, large load, long duration of flight and good invisibility performance, which has received the general attention of all countries in the world[2-4].

The cruising altitude of the stratospheric airship is generally between 18—20 km. The air density in this altitude layer is only 7%—8% of the sea level value. Hence, the attitude control ability of traditional aerodynamic control surface is reduced[5]. To solve this problem, some scholars have proposed a method for attitude control by changing the vehicle's centroid position, which is called moving mass control (MMC)[6-7]. Gao and Shan[8] proved that the centroid control of stratospheric airship is more advantageous than the one of aerodynamic control surface at stratospheric altitude. For most stratospheric airships, simplest MMC is carried out by adjusting the volume of ballonet. Nevertheless, due to the slow charging process, this method can't provide a fast response to the attitude control, and is easy to change the buoyancy, so it is more suitable for attitude fine-tuning control. With the development of MMC technology, an efficient MMC method was designed to change interior structure of airship by moving the liquid or solid payload, and has been verified in flight experiments[9-10]. For engineering reasons, the MMC method based on solid payload is more superior than the liquid one due to the better environmental adaptability and less additional weight to install. Especially, the total mass of the airship can be considered invariable when choosing part of the existing energy equipment as solid payload. In the current published literature, the dynamic model and handling characteristics of typical moving-mass stratospheric airship were provided[11-12], from which the scholars mainly focused on the attitude control ability and static trim method of the moving-mass actuator. Chen et al.[13] proposed a composite control strategy based on moving-mass actuator and aerodynamic control surface, which was first reported publicly in the field of stratospheric airships. However, the response process of the actuator was simplified as a motion with constant speed for simulation. As a matter of fact, the dynamic response capability

Received: 2021-10-08 **Accepted:** 2021-11-19
Foundation item: the National Natural Science Foundation of China (No. 51205253)
∗**E-mail:** quanbaowang@sjtu.edu.cn

of MMC actuator should be taken into consideration due to its strong time-delay and coupling characteristics. Therefore, it is of practical significance to study the attitude control ability under the dynamic response of moving-mass actuator.

In this paper, by taking the energy equipment as the mass slider. First, a design method of moving-mass stratospheric airship with constant total mass was presented, and a general dynamics equation was derived. Then, a position tracking controller of slider with input and state constraints was designed and the dynamic response parameters of the slider were obtained. Finally, the longitudinal motion simulation of stratospheric airship under dynamic response of the slider was established. From the open loop and closed loop controls respectively, the attitude control response and coupling characteristics were analyzed and compared with the ones of elevator.

Note: Unless otherwise specified, all vector parameters are expressed in the airship coordinate system, i.e. $(x,y,z)^{\mathrm{T}}=x\boldsymbol{i}+y\boldsymbol{j}+z\boldsymbol{k}$, where $\boldsymbol{i},\boldsymbol{j},\boldsymbol{k}$ are unit vectors along the airship axial (front), lateral (right) and vertical (bottom) directions respectively, which meet the right-hand rule.

1 Problem Description

The centroid position and rotational inertia of the stratospheric airship are no longer fixed under the change of internal structure. In addition, when the slider moves, it also has a corresponding coupling effect on the state parameters of the airship, which is mainly reflected in the following aspects.

1.1 Influence on Centroid and Rotational Inertia

Assuming that n energy equipment original located in the position of gondola $\boldsymbol{R}_{\mathrm{p}}=(x_{\mathrm{p}},y_{\mathrm{p}},z_{\mathrm{p}})^{\mathrm{T}}$ can be transformed to sliders with mass of $m_1,m_2,\cdots,m_n$ respectively, the new position of each slider is $\boldsymbol{R}_i=(x_i,y_i,z_i)^{\mathrm{T}}$, $i=1,2,\cdots,n$. Ignoring the mass of sliding rail, the airship body mass without sliders is expressed as $m_{\mathrm{B}}=m-\sum_{i=1}^{n}m_i$, where $m$denotes the total mass of the airship. According to the centroid theorem, the body and entire centroid of airship can be defined as

$$\left.\begin{aligned}\boldsymbol{R}_{\mathrm{B}}&=\begin{bmatrix}x_{\mathrm{B}}\\y_{\mathrm{B}}\\z_{\mathrm{B}}\end{bmatrix}=\frac{\boldsymbol{R}_{\mathrm{G0}}-\sum_{i=1}^{n}\mu_i\boldsymbol{R}_{\mathrm{p}}}{1-\sum_{i=1}^{n}\mu_i}\\ \boldsymbol{R}_{\mathrm{G}}&=\begin{bmatrix}x_{\mathrm{G}}\\y_{\mathrm{G}}\\z_{\mathrm{G}}\end{bmatrix}=\boldsymbol{R}_{\mathrm{G0}}-\sum_{i=1}^{n}\mu_i\boldsymbol{R}_{\mathrm{p}}+\sum_{i=1}^{n}\mu_i\boldsymbol{R}_i\end{aligned}\right\},\quad(1)$$

where $\mu_i=m_i/m$, $i=1,2,\cdots,n$ denotes the proportion of the slider in the total mass, and $\boldsymbol{R}_{\mathrm{G0}}$ denotes the original mass center of the airship. The rotational inertia of airship changes following with the position of slider, which can be deduced as

$$\begin{bmatrix}I_x\\I_y\\I_z\\I_{xy}\\I_{yz}\\I_{xz}\end{bmatrix}=\begin{bmatrix}I_{x_0}-\sum_{i=1}^{n}m_i(y_{\mathrm{p}}^2+z_{\mathrm{p}}^2)+\sum_{i=1}^{n}m_i(y_i^2+z_i^2)\\I_{y_0}-\sum_{i=1}^{n}m_i(x_{\mathrm{p}}^2+z_{\mathrm{p}}^2)+\sum_{i=1}^{n}m_i(x_i^2+z_i^2)\\I_{z_0}-\sum_{i=1}^{n}m_i(x_{\mathrm{p}}^2+y_{\mathrm{p}}^2)+\sum_{i=1}^{n}m_i(x_i^2+y_i^2)\\I_{xy_0}-\sum_{i=1}^{n}m_ix_{\mathrm{p}}y_{\mathrm{p}}+\sum_{i=1}^{n}m_ix_iy_i\\I_{yz_0}-\sum_{i=1}^{n}m_iy_{\mathrm{p}}z_{\mathrm{p}}+\sum_{i=1}^{n}m_iy_iz_i\\I_{xz_0}-\sum_{i=1}^{n}m_ix_{\mathrm{p}}z_{\mathrm{p}}+\sum_{i=1}^{n}m_ix_iz_i\end{bmatrix},\quad(2)$$

where $I_{x_0},I_{y_0},I_{z_0},I_{xy_0},I_{yz_0}$, and I_{xz_0} denote the original rotational inertia.

1.2 Influence on Centroid Velocity

The velocity of body centroid and mass sliders relative to inertial coordinate system can be written as

$$\left.\begin{aligned}&\boldsymbol{V}_{\mathrm{B}}=\boldsymbol{V}_0+\boldsymbol{\omega}\times\boldsymbol{R}_{\mathrm{B}}\\&\boldsymbol{V}_i=\boldsymbol{V}_0+\boldsymbol{\omega}\times\boldsymbol{R}_i+\dot{\boldsymbol{R}}_i\\&i=1,2,\cdots,n\end{aligned}\right\},\quad(3)$$

where $\boldsymbol{V}_0=(u,v,w)^{\mathrm{T}}$ denotes the velocity of the body-centred $\boldsymbol{O}_{\mathrm{b}}$ relative to inertial coordinate system, $\boldsymbol{\omega}=(p,q,r)^{\mathrm{T}}$ denotes the angular velocity vector of airship rotating around $\boldsymbol{O}_{\mathrm{b}}$, and $\dot{\boldsymbol{R}}_i=\partial\boldsymbol{R}_i/\partial t$ is the velocity of each mass slider relative to $\boldsymbol{O}_{\mathrm{b}}$. According to the velocity composition theorem, the velocity of entire centroid relative to inertial coordinate system can be written as

$$\boldsymbol{V}_{\mathrm{G}}=\boldsymbol{V}_0+\boldsymbol{\omega}^{\times}\boldsymbol{R}_{\mathrm{G}}+\sum_{i=1}^{n}\mu_i\dot{\boldsymbol{R}}_i,\quad(4)$$

$$\boldsymbol{\omega}^{\times}=\begin{bmatrix}0&-r&q\\r&0&-p\\-q&p&0\end{bmatrix},$$

where $\boldsymbol{\omega}^{\times}$ is the cross multiplication matrix of angular velocity vector.

1.3 Additional Force and Moment of Slider

According to Newton's second law in inertial coordinate system[14-16], the expression of entire centroid

dynamic equation in body coordinate system is

$$\left.\begin{aligned}&\boldsymbol{F}=m\frac{\mathrm{d}\boldsymbol{V}_{\mathrm{G}}}{\mathrm{d}t}\\&\boldsymbol{L}=\int_{\nabla}\boldsymbol{r}_i\times\mathrm{d}\boldsymbol{F}_i=\\&\qquad\int_{\mathrm{B}}\boldsymbol{r}_i\times\mathrm{d}\boldsymbol{F}_i+\sum_{i=1}^{n}\boldsymbol{R}_i\times m_i\frac{\mathrm{d}\boldsymbol{V}_i}{\mathrm{d}t}\end{aligned}\right\},\tag{5}$$

where $\boldsymbol{F}$ and $\boldsymbol{L}$ denote the resultant external force and moment of the airship respectively, $\mathrm{d}\boldsymbol{V}_{\mathrm{G}}/\mathrm{d}t$ and $\mathrm{d}\boldsymbol{V}_i/\mathrm{d}t$ are the absolute derivatives of the entire centroid velocity and the slider velocity of the airship to time, respectively, $\mathrm{d}\boldsymbol{F}_i$ denotes the external force on the mass element, $\boldsymbol{r}_i$ denotes the radius vector of $\mathrm{d}\boldsymbol{F}_i$, $\int_{\nabla}(\cdot)$ denotes the integral of element in the whole airship system, and $\int_{\mathrm{B}}(\cdot)$ denotes the integral in airship body only. Based on the vector derivative law, there are

$$\left.\begin{aligned}&\frac{\mathrm{d}\boldsymbol{V}_{\mathrm{G}}}{\mathrm{d}t}=\dot{\boldsymbol{V}}_{\mathrm{G}}+\boldsymbol{\omega}\times\boldsymbol{V}_{\mathrm{G}}\\&\frac{\mathrm{d}\boldsymbol{V}_i}{\mathrm{d}t}=\dot{\boldsymbol{V}}_i+\boldsymbol{\omega}\times\boldsymbol{V}_i\\&i=1,2,\cdots,n\end{aligned}\right\}.\tag{6}$$

The following dynamical equations can be derived from Eqs. (3)—(6):

$$\left.\begin{aligned}&\boldsymbol{F}=m[\dot{\boldsymbol{V}}_0+\dot{\boldsymbol{\omega}}^{\times}\boldsymbol{R}_{\mathrm{G}}+\boldsymbol{\omega}^{\times}\dot{\boldsymbol{R}}_{\mathrm{G}}+\sum_{i=1}^{n}\mu_i\ddot{\boldsymbol{R}}_i+\\&\boldsymbol{\omega}^{\times}(\boldsymbol{V}_0+\boldsymbol{\omega}^{\times}\boldsymbol{R}_{\mathrm{G}}+\textstyle\sum_{i=1}^{n}\mu_i\dot{\boldsymbol{R}}_i)]\\&\boldsymbol{L}=\boldsymbol{I}_0\dot{\boldsymbol{\omega}}+\boldsymbol{\omega}^{\times}(\boldsymbol{I}_0\boldsymbol{\omega})+m\boldsymbol{R}_{\mathrm{G}}^{\times}(\dot{\boldsymbol{V}}_0+\boldsymbol{\omega}^{\times}\boldsymbol{V}_0)+\\&\sum_{i=1}^{n}m_i\boldsymbol{R}_i^{\times}(2\boldsymbol{\omega}^{\times}\dot{\boldsymbol{R}}_i+\ddot{\boldsymbol{R}}_i)\end{aligned}\right\},\tag{7}$$

where $\boldsymbol{I}_0$ denotes the rotational inertia matrix of the airship (including mass slider) relative to $\boldsymbol{O}_{\mathrm{b}}$, and its value varies with the position of slider. $\boldsymbol{R}_{\mathrm{G}}^{\times}$ and $\boldsymbol{R}_i^{\times}(i=1,2,\cdots,n)$ are the cross multiplication matrices of the entire centroid and mass slider position of the airship, respectively.

Define $\boldsymbol{x}=(\boldsymbol{V}_0,\boldsymbol{\omega})^{\mathrm{T}}$ as the state variable of the airship, $\boldsymbol{x}_i=(\boldsymbol{R}_i,\dot{\boldsymbol{R}}_i,\ddot{\boldsymbol{R}}_i)^{\mathrm{T}}$, $i=1,2,\cdots,n$ as the state variable of sliders, then Eq. (7) can be written as

$$\begin{aligned}&\boldsymbol{M}(\boldsymbol{R}_i)\dot{\boldsymbol{x}}=\boldsymbol{f}(\boldsymbol{x},\boldsymbol{R}_i,\boldsymbol{U})+\boldsymbol{P}_{\mathrm{m}}(\boldsymbol{x},\boldsymbol{x}_i),\\&i=1,2,\cdots,n,\end{aligned}\tag{8}$$

where $\boldsymbol{M}(\boldsymbol{R}_i)$ denotes the additional mass matrix varying with the slider position, $\boldsymbol{f}(\boldsymbol{x},\boldsymbol{R}_i,\boldsymbol{U})$ denotes the nonlinear force and moment terms driven by input $\boldsymbol{U}$, which is composed of thrust $\boldsymbol{T}$, aerodynamic $\boldsymbol{A}$, inertial $\boldsymbol{I}$, buoyancy $\boldsymbol{B}$ and gravity $\boldsymbol{G}$. $\boldsymbol{P}_{\mathrm{m}}(\boldsymbol{x},\boldsymbol{x}_i)$, $i=1,2,\cdots,n$ denotes the additional force and moment exerted on airship by sliders. The expression can be obtained according to Eq. (7):

$$\boldsymbol{P}_{\mathrm{m}}=-\begin{bmatrix}\sum_{i=1}^{n}m_i(\ddot{\boldsymbol{R}}_i+2\boldsymbol{\omega}^{\times}\dot{\boldsymbol{R}}_i)\\\sum_{i=1}^{n}m_i\boldsymbol{R}_i^{\times}(\ddot{\boldsymbol{R}}_i+2\boldsymbol{\omega}^{\times}\dot{\boldsymbol{R}}_i)\end{bmatrix}.\tag{9}$$

When $\dot{\boldsymbol{R}}_i=\ddot{\boldsymbol{R}}_i=0$, $i=1,2,\cdots,n$, there is no relative motion between sliders and airship, and the additional term $\boldsymbol{P}_{\mathrm{m}}=\boldsymbol{0}$. Thus, the relationship between flight attitude and slider position presents a static coupling characteristic. For another situation, when the slider is controllable and moves relative to the airship, $\boldsymbol{P}_{\mathrm{m}}$ becomes time-varying, and its value is determined by command response capability of the slider. Therefore, the influence of slider control response process on airship motion state should be considered.

2 Parametric Modeling

2.1 Design of Moving-Mass Mechanism

Considering that the standard motion attitude of stratospheric airship is $\phi=\theta=0$, the centroid moment of airship near the standard attitude can be deduced as

$$\boldsymbol{L}_{\mathrm{G}}=\boldsymbol{R}_{\mathrm{G}}\times\boldsymbol{G}=(y_{\mathrm{G}}G,-x_{\mathrm{G}}G,0)^{\mathrm{T}},\tag{10}$$

where $G=mg$ represents the gravity value of the airship, and constant g is the gravitational acceleration.

This shows that MMC method can achieve the control of pitch and roll torque, but cannot directly change the yaw torque. In addition, since the centroid of the airship is located below the body-centred and in the symmetric plane, the airship is self-stable in the rolling direction. Thus, there was no need to control roll torque without external disturbance. For streamline stratospheric airship, the inner surface at the bottom of the envelope is the best choice to install MMC mechanism, which can provide a large sliding space for sliders in the axial direction. The centroid component x_{G} varies greatly with the position of the slider, and brings a good operation ability in the pitch direction, which has practical engineering significance. In this paper, the 250 m high altitude airship (HAA) in the United States is taken as the research object, and the original parameters are derived from Ref. [17]. The key parameters are listed in Table 1.

Suppose there is a sliding rail L parallel to the longitudinal axis with a length of 100m installed at the inner surface of the bottom of the envelope, and its center position is at the maximum diameter of the envelope. One energy equipment with mass of m_{L} from the position of gondola $\boldsymbol{R}_{\mathrm{p}}=(x_{\mathrm{p}},y_{\mathrm{p}},z_{\mathrm{p}})^{\mathrm{T}}$ is transferred to the sliding rail L as a slider, which can slide freely on the rail L.

Table 1 Original airship parameters

Parameter	Value	Unit	Remark
m	5.6×10^4	kg	Total mass
∇	7.4×10^5	m^3	Volume
L	250	m	Length
D	75	m	Max diameter
$\boldsymbol{R}_{\mathrm{G}_0}=(x_{\mathrm{G}_0},y_{\mathrm{G}_0},z_{\mathrm{G}_0})^{\mathrm{T}}$	$(0,0,15)^{\mathrm{T}}$	m	Original entire centroid
$\boldsymbol{R}_{\mathrm{p}}=(x_{\mathrm{p}},y_{\mathrm{p}},z_{\mathrm{p}})^{\mathrm{T}}$	$(0,0,40)^{\mathrm{T}}$	m	Gondola position
$\boldsymbol{R}_{\mathrm{T}}=(x_{\mathrm{T}},\pm y_{\mathrm{T}},z_{\mathrm{T}})^{\mathrm{T}}$	$(0,\pm5,40)^{\mathrm{T}}$	m	Left (right) vectored thruster position
I_{x_0}	5×10^7	$\mathrm{kg}\cdot\mathrm{m}^2$	
I_{y_0}	2.9×10^8	$\mathrm{kg}\cdot\mathrm{m}^2$	Original rotational inertia
I_{z_0}	2.9×10^8	$\mathrm{kg}\cdot\mathrm{m}^2$	$I_{xy_0}=I_{yz_0}=0$
I_{xz_0}	-6×10^8	$\mathrm{kg}\cdot\mathrm{m}^2$	
k_{a}	0.17	—	
k_{b}	0.83	—	Added mass coefficients
k_{c}	0.52	—	

Figure 1 shows the definition of coordinate systems and the structure diagram of moving-mass airship.

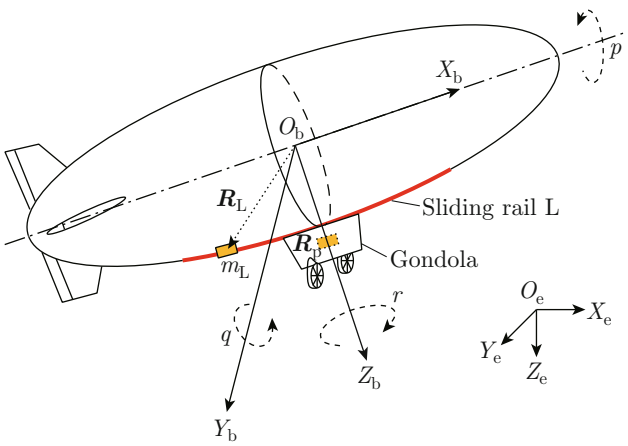

Fig. 1 Structure diagram of moving-mass airship

For simplification, the rail L can be approximately equivalent to a straight segment parallel to the coordinate axis X_{b} if the envelope of the airship is enough large. The slider parameters can be obtained as follow:

$$\left.\begin{aligned}\boldsymbol{R}_{\mathrm{L}}&=(x_{\mathrm{L}},y_{\mathrm{L}},z_{\mathrm{L}})^{\mathrm{T}}=(X_{\mathrm{L}},0,b)^{\mathrm{T}}\\ \dot{\boldsymbol{R}}_{\mathrm{L}}&=(\dot{x}_{\mathrm{L}},\dot{y}_{\mathrm{L}},\dot{z}_{\mathrm{L}})^{\mathrm{T}}=(\dot{X}_{\mathrm{L}},0,0)^{\mathrm{T}}\\ \ddot{\boldsymbol{R}}_{\mathrm{L}}&=(\ddot{x}_{\mathrm{L}},\ddot{y}_{\mathrm{L}},\ddot{z}_{\mathrm{L}})^{\mathrm{T}}=(\ddot{X}_{\mathrm{L}},0,0)^{\mathrm{T}}\end{aligned}\right\},\tag{11}$$

where $X_{\mathrm{L}},\dot{X}_{\mathrm{L}},\ddot{X}_{\mathrm{L}}$ represent the displacement, velocity and acceleration of slider relative to the center of sliding rail, respectively. $b=D/2$, where D denotes the maximum diameter of envelope. The additional force and moment terms from Eq. (9) can be rewritten as

$$\begin{aligned}\boldsymbol{P}_{\mathrm{m}}=&-m_{\mathrm{L}}\begin{bmatrix}\ddot{\boldsymbol{R}}_{\mathrm{L}}+2\boldsymbol{\omega}^{\times}\dot{\boldsymbol{R}}_{\mathrm{L}}\\ \boldsymbol{R}_{\mathrm{L}}^{\times}(\ddot{\boldsymbol{R}}_{\mathrm{L}}+2\boldsymbol{\omega}^{\times}\dot{\boldsymbol{R}}_{\mathrm{L}})\end{bmatrix}=\\ &-m_{\mathrm{L}}\begin{bmatrix}\ddot{X}_{\mathrm{L}}\\ 2rX_{\mathrm{L}}\\ -2q\dot{X}_{\mathrm{L}}\\ -2br\dot{X}_{\mathrm{L}}\\ b\ddot{X}_{\mathrm{L}}+2qX_{\mathrm{L}}\dot{X}_{\mathrm{L}}\\ 2rX_{\mathrm{L}}\dot{X}_{\mathrm{L}}\end{bmatrix}.\end{aligned}\tag{12}$$

It is obvious that the motion of the slider is coupled to each channel. Fortunately, it can be decoupled from the longitudinal motion ($v=p=r=\beta=0$). Based on this, the coupling characteristics of the slider can be analyzed from the longitudinal motion of the airship.

2.2 Longitudinal Motion Equation

Without considering external disturbance, the longitudinal motion equation of airship can be decoupled by Eq. (8). The affine nonlinear form is as follows:

$$\begin{aligned}\boldsymbol{M}_{\mathrm{L}}(X_{\mathrm{L}})\dot{\boldsymbol{x}}_{\mathrm{L}}=&\boldsymbol{f}_{\mathrm{L}}(\boldsymbol{x}_{\mathrm{L}},X_{\mathrm{L}},\dot{X}_{\mathrm{L}},\ddot{X}_{\mathrm{L}},\theta)+\\ &\boldsymbol{B}_{\mathrm{L}}(\boldsymbol{x}_{\mathrm{L}})\boldsymbol{U}_{\mathrm{L}},\end{aligned}\tag{13}$$

where $\boldsymbol{x}_{\mathrm{L}}=(u,w,q)^{\mathrm{T}}$ denotes the longitudinal state variables, and $\boldsymbol{U}_{\mathrm{L}}=(T_x,T_z,\delta_{\mathrm{e}})^{\mathrm{T}}$ denotes the control input of trust and elevator. Other parameters are as follows:

(1) Additional mass matrix:

$$\boldsymbol{M}_{\mathrm{L}}(X_{\mathrm{L}})=\begin{bmatrix} m+m_{11} & 0 & mz_{\mathrm{G}} \\ 0 & m+m_{33} & -mx_{\mathrm{G}} \\ mz_{\mathrm{G}} & -mx_{\mathrm{G}} & I_y+m_{55} \end{bmatrix}, \quad (14)$$

$$\begin{aligned} \text{s.t.}\ \ & x_{\mathrm{G}}=x_{\mathrm{G}_0}+\mu_{\mathrm{L}}(X_{\mathrm{L}}-x_{\mathrm{p}}), \\ & z_{\mathrm{G}}=z_{\mathrm{G}_0}-\mu_{\mathrm{L}}z_{\mathrm{p}}, \\ & I_y=I_{y_0}+m_{\mathrm{L}}(X_{\mathrm{L}}^2+b^2-z_{\mathrm{p}}^2). \end{aligned}$$

(2) Nonlinear term:

$$\boldsymbol{f}_{\mathrm{L}}(\boldsymbol{x}_{\mathrm{L}},X_{\mathrm{L}},\dot{X}_{\mathrm{L}},\ddot{X}_{\mathrm{L}},\theta)=\begin{bmatrix} mx_{\mathrm{G}}q^2-(m+m_{33})wq+(B-G)\sin\theta+X_{\mathrm{AL0}}-m_{\mathrm{L}}\ddot{X}_{\mathrm{L}} \\ (m+m_{11})uq+mz_{\mathrm{G}}q^2+(G-B)\cos\theta+W_{\mathrm{AL0}}+2m_{\mathrm{L}}q\dot{X}_{\mathrm{L}} \\ -mx_{\mathrm{G}}uq-mz_{\mathrm{G}}wq-x_{\mathrm{G}}G\cos\theta-z_{\mathrm{G}}G\sin\theta+M_{\mathrm{AL0}}-2m_{\mathrm{L}}qX_{\mathrm{L}}\dot{X}_{\mathrm{L}}-bm_{\mathrm{L}}\ddot{X}_{\mathrm{L}} \end{bmatrix}, \quad (15)$$

where B denotes the buoyancy value of the airship.

(3) Control coefficient matrix:

$$\boldsymbol{B}_{\mathrm{L}}(\boldsymbol{x}_{\mathrm{L}})=\begin{bmatrix} 1 & 0 & Q_\infty S_{\mathrm{ref}}(-C_x^{\delta_{\mathrm{e}}}\cos\alpha+C_z^{\delta_{\mathrm{e}}}\sin\alpha) \\ 0 & 1 & Q_\infty S_{\mathrm{ref}}(-C_x^{\delta_{\mathrm{e}}}\sin\alpha-C_z^{\delta_{\mathrm{e}}}\cos\alpha) \\ z_{\mathrm{T}} & -x_{\mathrm{T}} & Q_\infty\nabla C_{\mathrm{m}}^{\delta_{\mathrm{e}}} \end{bmatrix}. \quad (16)$$

In Eqs. (14)—(16), $x_{\mathrm{G}}, z_{\mathrm{G}}$ denote the coordinate components of centroid, $Q_\infty=0.5\rho_{\mathrm{air}}V_{\mathrm{a}}^2$ is the dynamic pressure, ρ_{air} denotes the air density, $V_{\mathrm{a}}=\sqrt{u_{\mathrm{a}}^2+w_{\mathrm{a}}^2}$ denotes the airspeed, $\alpha=\tan^{-1}(w_{\mathrm{a}}/u_{\mathrm{a}})$ denotes the attack angle, $S_{\mathrm{ref}}=\nabla^{2/3}$ denotes the reference area of airship, ∇ is the volume of envelope, $C_x^{\delta_{\mathrm{e}}}\approx 0$, $C_z^{\delta_{\mathrm{e}}}=0.16$, $C_{\mathrm{m}}^{\delta_{\mathrm{e}}}=-0.21$ denote the coefficients of elevator, $x_{\mathrm{T}}, z_{\mathrm{T}}$ are the coordinate components of vectored thruster, and $X_{\mathrm{AL0}}, W_{\mathrm{AL0}}, M_{\mathrm{AL0}}$ represent the aerodynamic force and moment independent of input parameters in forward, vertical and pitching directions, respectively. According to the definition of aerodynamic force in Ref. [18], these terms can be deduced that:

$$\left.\begin{aligned} X_{\mathrm{AL0}} &= Q_\infty S_{\mathrm{ref}}[-(C_{x0}+C_x^\alpha\alpha)\cos\alpha+ \\ &\quad (C_{z0}+C_z^\alpha\alpha)\sin\alpha] \\ W_{\mathrm{AL0}} &= Q_\infty S_{\mathrm{ref}}[-(C_{x0}+C_x^\alpha\alpha)\sin\alpha- \\ &\quad (C_{z0}+C_z^\alpha\alpha)\cos\alpha] \\ M_{\mathrm{AL0}} &= Q_\infty\nabla(C_{\mathrm{m}}^\alpha\alpha+C_{\mathrm{m}}^{\dot\alpha}\dot\alpha+C_{\mathrm{m}}^q q) \end{aligned}\right\}, \quad (17)$$

where $C_{x0}, C_{z0}, C_x^\alpha, C_z^\alpha, C_{\mathrm{m}}^\alpha, C_{\mathrm{m}}^{\dot\alpha}$ and C_{m}^q are the aerodynamic coefficients of the airship.

3 Slider Controller Design

The dynamic response of the aerodynamic control surface can be expressed by a first-order transfer function. Taking the elevator as an example:

$$\delta_{\mathrm{e}}(S)=\frac{1}{T_\delta S+1}\delta_{\mathrm{ed}}(S), \quad (18)$$

where δ_{ed} denotes the desired control input of elevator, δ_{e} denotes the actual output of the actuator, S is the frequency domain parameter, and T_δ is the temporal response constant. The dynamic process is usually ignored in that the response time of such actuator is much shorter than each motion mode of the airship. By comparison, the low control frequency, obvious dynamic response process and coupling influence of MMC mechanism make the control response process shall be taken into consideration.

3.1 Tracking Control Model

In this paper, the slider is regarded as a position tracking control subsystem, and the controller is designed independently to let the output X_{L} tracking the desired signal $X_{\mathrm{Ld}}(\dot{X}_{\mathrm{Ld}}=\ddot{X}_{\mathrm{Ld}}=0)$. Let $\ddot{X}_{\mathrm{L}}$ be the control input of the slider, and the state variables are $X_{\mathrm{L}}, \dot{X}_{\mathrm{L}}$. Assuming that the state of the slider is observable, then the linear tracking error feedback control law can be designed as

$$u_{\mathrm{c}}=k_1e_{\mathrm{L}}+k_2\dot{e}_{\mathrm{L}}, \quad (19)$$

where $e_{\mathrm{L}}=X_{\mathrm{Ld}}-X_{\mathrm{L}}$ is the position tracking error of the slider. Its first derivative $\dot{e}_{\mathrm{L}}=\dot{X}_{\mathrm{Ld}}-\dot{X}_{\mathrm{L}}=-\dot{X}_{\mathrm{L}}$ denotes the velocity tracking error, its second derivative $\ddot{e}_{\mathrm{L}}=\ddot{X}_{\mathrm{Ld}}-\ddot{X}_{\mathrm{L}}=-\ddot{X}_{\mathrm{L}}$. k_1, k_2 are the control gain coefficients. Define tracking error state variable $\boldsymbol{E}=(e_{\mathrm{L}},\dot{e}_{\mathrm{L}})^{\mathrm{T}}$. Then, the state space expression of the tracking error system is

$$\begin{aligned} &\dot{\boldsymbol{E}}=\boldsymbol{A}\boldsymbol{E}+\boldsymbol{B}\ddot{X}_{\mathrm{L}}, \quad (20)\\ &\boldsymbol{A}=\begin{bmatrix}0&1\\0&0\end{bmatrix},\quad \boldsymbol{B}=\begin{bmatrix}0\\-1\end{bmatrix}. \end{aligned}$$

Actually, the input $\ddot{X}_{\mathrm{L}}$ is limited, so it can be expressed by the saturation function:

$$\ddot{X}_{\mathrm{L}}=\mathrm{sat}(u_{\mathrm{c}})=\mathrm{sat}(\boldsymbol{K}\boldsymbol{E}),\quad \boldsymbol{K}=(k_1,k_2), \quad (21)$$

where $\boldsymbol{K}_{1\times 2}$ denotes the feedback matrix, and the saturation function is defined as

$$\mathrm{sat}(u_{\mathrm{c}})=\mathrm{sign}(u_{\mathrm{c}})\min(u_{\max},|u_{\mathrm{c}}|), \quad (22)$$

where $u_{\max}$ denotes the limit of input, then the closed-loop form of the error system is

$$\dot{\boldsymbol{E}} = \boldsymbol{A}\boldsymbol{E} + \boldsymbol{B}\mathrm{sat}(\boldsymbol{K}\boldsymbol{E}). \tag{23}$$

The linear control region can be determined by $\boldsymbol{K}$:

$$\mathcal{L}(\boldsymbol{K} = \{\boldsymbol{E} \in \mathbf{R}^2 : |\boldsymbol{K}\boldsymbol{E}| \leqslant u_{\max}\}. \tag{24}$$

3.2 Stability Analysis with Input Constraints

According to the definition of asymptotically null controllable with bounded controls (ANCBC)[19], if satisfied: $(\boldsymbol{A}, \boldsymbol{B})$ is stabilizable; $\lambda(\boldsymbol{A}) \subset \mathbb{C}^- \cup \mathbb{C}^0$, the global stabilization of the system is possible even if the input is limited. $\lambda(\boldsymbol{A})$ denotes the set of all the eigenvalues of $\boldsymbol{A}$, $\mathbb{C}^-$ denotes the open left-half complex plane, and $\mathbb{C}^0$ denotes the imaginary axis in the complex plane.

Obviously, system (23) is an ANCBC system with $\lambda(\boldsymbol{A}) = \pm i \subset \mathbb{C}^- \cup \mathbb{C}^0$ and $\mathrm{rank}(\boldsymbol{A}\boldsymbol{B}, \boldsymbol{A}) = 2$. If $\boldsymbol{A} + \boldsymbol{B}\boldsymbol{K}$ is Hurwitz stable, the eigenvalues of $\boldsymbol{A} + \boldsymbol{B}\boldsymbol{K}$ should be satisfied:

$$\lambda(\boldsymbol{A} + \boldsymbol{B}\boldsymbol{K}) = \lambda_{1,2} = \frac{-k_2 \pm \sqrt{k_2^2 - 4k_1}}{2} \subset \mathbb{C}^-. \tag{25}$$

Thus, if k_1, k_2 meet the condition in Eq. (25), the final stability of the error system can be realized, even if the error system may appear in the nonlinear saturation region, it will turn back to the linear control region and tend to be stable, as shown in Fig. 2, where $\boldsymbol{S}(\boldsymbol{E}_0)$ is the initial state region, and $\boldsymbol{\Phi}(t, \boldsymbol{E}_0)$ is the solution at the time of t from the initial state $\boldsymbol{E}_0$.

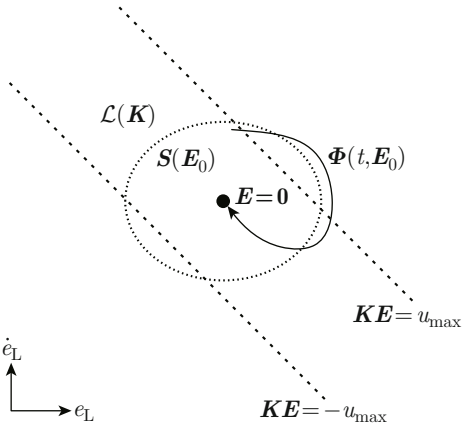

Fig. 2 Description of saturation control for ANCBC system

3.3 Constraint Processing

Assuming the sliding rail is smooth, the control structure of the slider subsystem is shown as follows:

From Fig. 3, the desired position X_{Ld} and velocity of

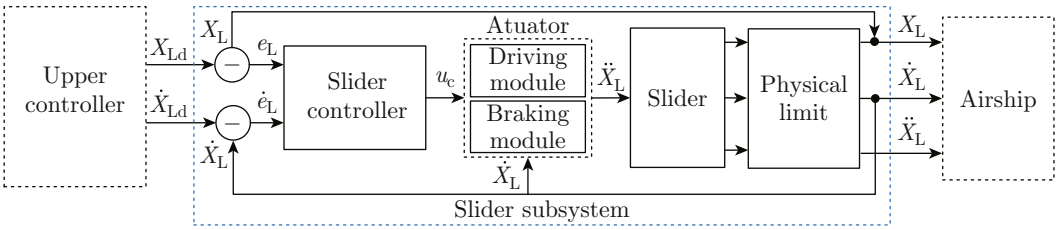

Fig. 3 Structure drawing of slider controller

slider $\dot{X}_{\mathrm{Ld}}$ can be solved by the upper controller. The actuator of the slider subsystem is divided into driving and braking modules, which are worked in acceleration and deceleration processes respectively. Physical limit is a constraint on the motion range of slider, satisfying the following conditions:

$$\left.\begin{aligned} &\text{if} \quad X_{\mathrm{L}} \geqslant X_{\mathrm{L\_max}} \Rightarrow \begin{cases} X_{\mathrm{L}} = X_{\mathrm{L\_max}} \\ \dot{X}_{\mathrm{L}} = 0 \\ \ddot{X}_{\mathrm{L}} = 0 \end{cases} \\ &\text{elseif} \quad X_{\mathrm{L}} \leqslant -X_{\mathrm{L\_max}} \Rightarrow \begin{cases} X_{\mathrm{L}} = -X_{\mathrm{L\_max}} \\ \dot{X}_{\mathrm{L}} = 0 \\ \ddot{X}_{\mathrm{L}} = 0 \end{cases} \end{aligned}\right\}. \tag{26}$$

3.3.1 *Position Constraint Processing*

The motion of the slider will be cut-off when X_{L} exceeds the position limit $X_{\mathrm{L\_max}}$. In order to prevent this phenomenon cause by the overshoot of control response, let the desired signal $|X_{\mathrm{Ld}}| \leqslant X_{\mathrm{L\_max}}$, and the relationship between k_1, k_2 satisfy the condition of $k_2^2 \geqslant 4k_1 > 0$. Hence, the eigenvalues of $\boldsymbol{A} + \boldsymbol{B}\boldsymbol{K}$ will have no imaginary part. While in the linear control region $\mathcal{L}(\boldsymbol{K})$, the tracking error system will be worked as a second-order system with critical damping or overdamping characteristics, and can ensure $\forall t > 0$, $|X_{\mathrm{L}}(t)| \leqslant X_{\mathrm{L\_max}}$. Especially, when the tracking error system is critical damping ($k_2^2 = 4k_1$), it can take the shortest time to stabilize.

3.3.2 *Velocity Constraint Processing*

The velocity constraint of the slider can be expressed as $\left|\dot{X}_{\mathrm{L}}\right| \leqslant v_{\max}$. In order to deal with this constraint, the control of slider is divided into two case, which is judged by the sign of $u_{\mathrm{c}}\dot{X}_{\mathrm{L}}$.

(1) Case 1. If $u_{\mathrm{c}}\dot{X}_{\mathrm{L}} \geqslant 0$, the driving module works, which makes the slider speed up. Mark $u_{\mathrm{c}+}$ as the

control input produced by driving module, written as

$$u_{c+} = u_c \frac{\text{sign}(v_{\max} - \varepsilon - |\dot{X}_L|) + 1}{2}, \tag{27}$$

where $\varepsilon > 0$ is relatively small value. In this case, when $|\dot{X}_L| \to v_{\max}^-$, $u_{c+} = 0$, the velocity of slider keeps unchanged, unless breaking module works.

(2) Case 2. If $u_c \dot{X}_L < 0$, the breaking module works, which makes the slider slow down. Mark u_{c-} as the control input produced by breaking module, and $u_{c-} = u_c$.

Thus, the velocity of slider can be limited. The region of control cases and the change trend of the tracking error are shown in Fig. 4.

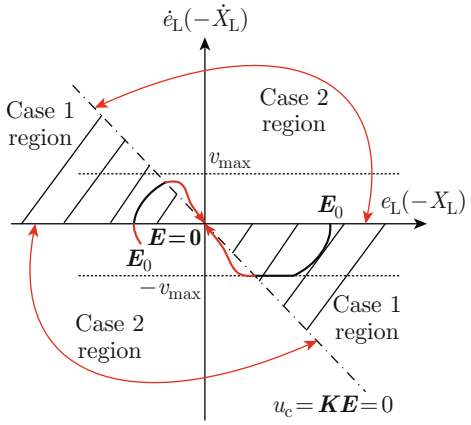

Fig. 4 Control cases and change trend of the tracking error

3.3.3 *Input Constraint Processing*

Considering the advantages of ANCBC system in control stability, the input saturation is allowed in the controller. In different cases, the input of slider can be expressed as

$$\left.\begin{aligned} \ddot{X}_L &= \text{sat}_+(u_{c+}), \quad \text{Case 1} \\ \ddot{X}_L &= \text{sat}_+(u_{c-}), \quad \text{Case 2} \end{aligned}\right\}. \tag{28}$$

The definition of saturation function is as follow:

$$\left.\begin{aligned} &\text{sat}_+(u_{c+}) = \text{sign}(u_{c+}) \cdot \min(u_{\text{Lmax}+}, |u_{c+}|) \\ &\text{sat}_-(u_{c-}) = \text{sign}(u_{c-}) \cdot \min(u_{\text{Lmax}-}, |u_{c-}|) \\ &\text{s.t.} \quad u_{\text{Lmax}+} = \min\left(\frac{\eta P}{m_L |\dot{X}_L|}, \bar{u}_{\text{drive}}\right) \end{aligned}\right\}, \tag{29}$$

where $u_{\text{Lmax}+}$ and $u_{\text{Lmax}-}$ are the driving and braking constraints of the slider respectively, P is the rated power of the driving motor, η is the conversion efficiency of electrical to mechanical energy, and $\bar{u}_{\text{drive}}$ is set to prevent the starting acceleration from being too large.

The controller design process of slider subsystem is shown in Fig. 5.

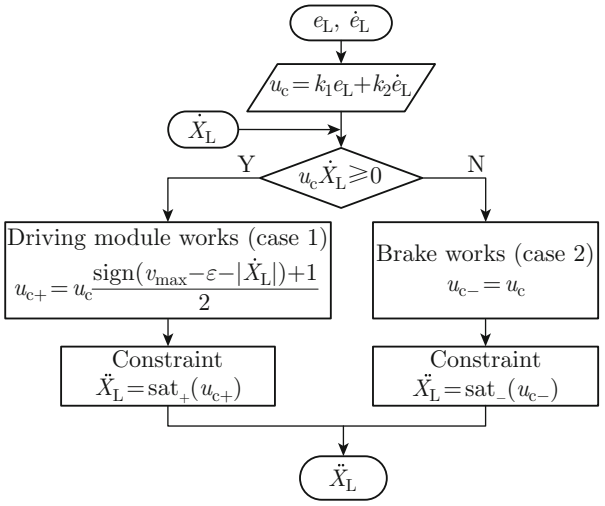

Fig. 5 Slider controller design process

3.4 Control Gain Coefficients Design

From Section 3.3, the relationship between k_1 and k_2 is identified. Thus, the feedback matrix can be expressed as $\boldsymbol{K}(k_1) = (k_1, 2\sqrt{k_1})$, $k_1 > 0$. Then, the linear control region $\mathcal{L}(\boldsymbol{K})$ can be adjusted by k_1. If the initial state region $\boldsymbol{S}(\boldsymbol{E}_0)$ is known, a conservative k_1 can be obtained to let $\boldsymbol{S}(\boldsymbol{E}_0) \subset \mathcal{L}(\boldsymbol{K})$, then the input saturation will be avoided as far as possible.

In this paper, set $\bar{u}_{\text{drive}} = 2\,\text{m/s}^2$, $X_{\text{L\_max}} = 50\,\text{m}$, $P = 20\,\text{kw}$, $\eta = 0.75$, $m_L = 2\,800\,\text{kg}$, $v_{\max} = 4\,\text{m/s}$. According to the position constraint, we can assume that $\boldsymbol{S}(\boldsymbol{E}_0) = \{\boldsymbol{E}_0 = (e_{L0}, 0)^T \in \mathbf{R}^2 \,|\, |e_{L0}| \leqslant 2X_{\text{L\_max}}\}$. Figure 6 shows the relationship between initial state and linear control region. When $k_1 = \dfrac{\bar{u}_{\text{drive}}}{2X_{\text{L\_max}}} = 0.02$, it can be ensured that the initial state region $\boldsymbol{S}(\boldsymbol{E}_0) \subset \mathcal{L}(\boldsymbol{K})$ completely.

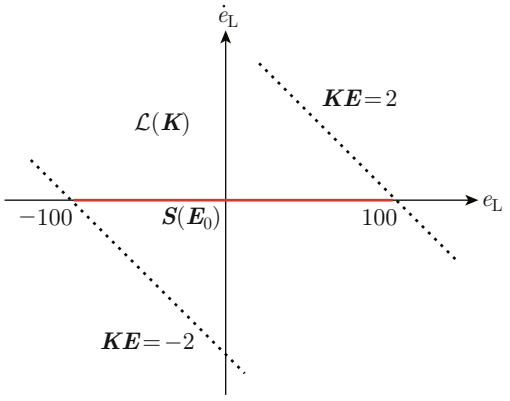

Fig. 6 Relationship between initial state and linear control region

Assuming that $X_L(0) = -50\,\text{m}$ and $X_{Ld} = 50\,\text{m}$, the step response of the sliding block control system with different control gain coefficients is shown in Fig. 7.

In Fig. 7(a), $k_2 = 2\sqrt{k_1}$ is fixed, which means the

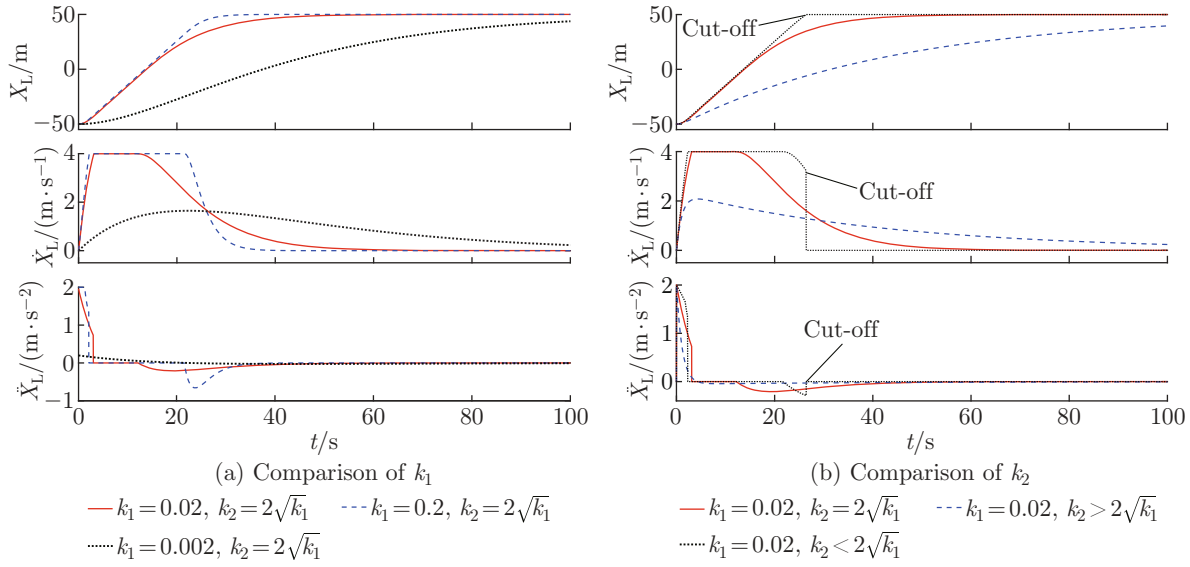

(a) Comparison of k_1 (b) Comparison of k_2

—$k_1=0.02,\ k_2=2\sqrt{k_1}$ - - -$k_1=0.2,\ k_2=2\sqrt{k_1}$ ·····$k_1=0.002,\ k_2=2\sqrt{k_1}$

—$k_1=0.02,\ k_2=2\sqrt{k_1}$ - - -$k_1=0.02,\ k_2>2\sqrt{k_1}$ ·····$k_1=0.02,\ k_2<2\sqrt{k_1}$

Fig. 7 Comparison of step response with different slider control gain coefficients

tracking error system is critical damping, there is no overshoot phenomenon in the step response, and the velocity constraint is handled well. The larger k_1 is, the faster control response will be, although the input saturation occurs. In Fig. 7(b), $k_1 = 0.02$ is fixed. When $k_2 < 2\sqrt{k_1}$, the system is underdamped, and the motion of slider is cut-off due to overshoot. When $k_2 > 2\sqrt{k_1}$, the system is overdamped, and has a poor response performance relative to the system with critical damping characteristics.

Therefore, it is reasonable to design the control gain coefficients by setting $k_2 = 2\sqrt{k_1}$, and the specific design of k_1 depends on the requirement of response performance in attitude control.

4 Attitude Control Simulation

4.1 Operation Ability Comparison

If the airship can keep a steady flight at zero attack angle with airspeed of V_A in the longitudinal plane. In such steady-state condition, the airship has no attitude rotation with $q = 0$, the longitudinal state variable keeps $\dot{\boldsymbol{x}}_L = \boldsymbol{0}$, and the slider is at a relatively static state with $\dot{X}_L = \ddot{X}_L = 0$. Assuming that the airship always keeps the float-weight balance with $B = G$, then, at steady state time, the relationship between control variables and state variables in longitudinal motion can be obtained by Eq. (13):

$$\left.\begin{aligned} &T_x - Q_\infty S_{\text{ref}}(C_{x0} + C_x^{\delta_e}\delta_e) = 0 \\ &T_z - Q_\infty S_{\text{ref}}(C_{z0} + C_z^{\delta_e}\delta_e) = 0 \\ &T_x z_T - T_z x_T + Q_\infty \nabla C_m^{\delta_e}\delta_e - \\ &\qquad x_G G\cos\theta - z_G G\sin\theta = 0 \end{aligned}\right\}. \tag{30}$$

In order to compare the attitude control ability of slider and elevator at different airspeeds and mass ratios of the slider, respectively, taking individual maximum control value, the pitching angle is calculated at the airspeed ranging from 0 to 30 m/s in the case of different mass ratios $\mu_L = m_L/m$. The comparison results are shown in Fig. 8.

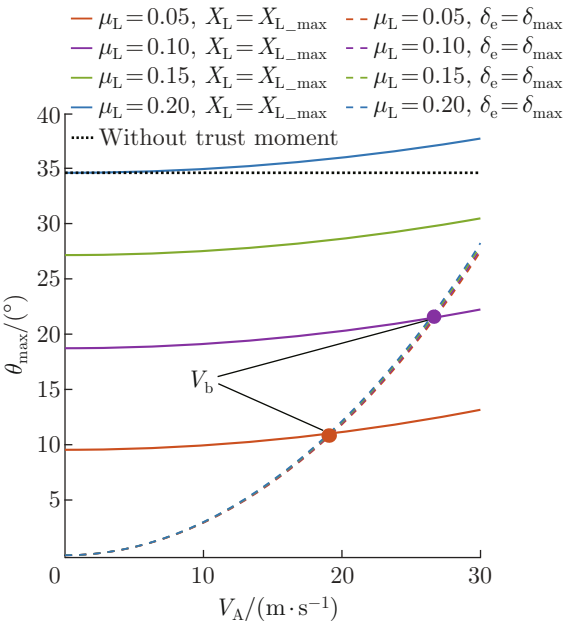

Fig. 8 Comparison of pitching angle operation ability between slider and elevator at different airspeeds and mass ratios

In Fig. 8, four real curves represent the relationship between the maximum pitching control ability of slider and airspeed, under different mass ratios of slider, respectively. It can be seen that the greater value

of μ_{L} brings the stronger pitching angle control ability of the slider. The upward trend of the curves is caused by the moment of thrust which is proportional to V_{A}^2. If the vector thrust is installed on both sides of the equatorial plane of the envelope, $z_{\mathrm{T}} = x_{\mathrm{T}} = 0$, the moment of thrust $\boldsymbol{L}_{\mathrm{Tm}} \equiv \boldsymbol{0}$, thus the pitching control ability of the slider will be a constant value $\theta_{\max} = \tan^{-1} \dfrac{x_{\mathrm{G0}} + \mu_{\mathrm{L}}(X_{\mathrm{L\_max}} - x_{\mathrm{p}})}{z_{\mathrm{G0}} - \mu_{\mathrm{L}} z_{\mathrm{p}}}$ at any airspeed, which is shown as a black straight line. Another four dotted curves represent the relationship between the maximum pitching control ability of elevator and airspeed, under different mass ratios of slider, respectively. It can be seen that the pitching control ability changes greatly at different airspeeds. The critical airspeed V_{b} at the intersection of two types of curves shows that in which situation the pitching operation capability of the two actuators are the same. When $V_{\mathrm{A}} < V_{\mathrm{b}}$, the pitching operation ability of the slider is greater than that of elevator, otherwise will be reversed. Furthermore, V_{b} increases as μ_{L} increases, and the relationship between μ_{L} and V_{b} is shown in Fig. 9.

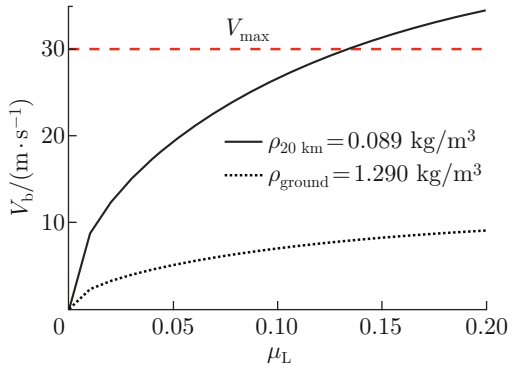

Fig. 9 Relationship between mass ratio μ_{L} and critical airspeed V_{b}

In Fig. 9, the two curves represent the variation ofV_{b} with μ_{L} in the near-surface (0 km) and stratospheric ($\sim$ 20 km) atmospheric environments, respectively. The velocity range in the upper half plane of the curve indicates that the operational capability of elevator is greater than that of the slider, otherwise will be reversed. Assuming the maximum airspeed $V_{\max} = 30\,\mathrm{m/s}$, it can be seen that in the stratospheric atmosphere, when $\mu_{\mathrm{L}} > 0.135$, $V_{\mathrm{b}} > V_{\max}$ which means that the operation ability of the slider in the whole airspeed range is greater than that of elevator, that is, the MMC method can completely replace the elevator for pitching angle control in the range of $\theta_{\max}$. While at the flight altitude near the ground, the value of V_{b} is generally small, the operational efficiency of the elevator is significantly improved, and the airspeed range is mostly located in the upper half of the curve. Thus, the composite attitude control can be considered.

4.2 Analysis of Attitude Control Response and Coupling

When the MMC mechanism is used for attitude control, it is necessary to associate the dynamic response performance of the slider with the coupling effect on airship. Based on the slider controller and MMC model designed above, under the initial conditions of $V_{\mathrm{a0}} = 20\,\mathrm{m/s}$, $\alpha_0 = 0$, $\theta_0 = 0$, the airship is controlled to track the desired pitching angle $\theta_{\mathrm{d}} = 10°$ by MMC method. During the control period, the elevator keeps zero and thrust is remained unchanged.

4.2.1 *Open-Loop Attitude Control Response*

The open-loop control of airship attitude does not require the feedback of airship state parameters, so the control value is determined by the expected attitude at the steady-state moment only. According to Eq. (30), the relationship between the steady-state control value $\bar{X}_{\mathrm{Ld}}$ which the slider needs to track and the desired pitching angle θ_{d} can be derived as follows:

$$\bar{X}_{\mathrm{Ld}} = \frac{C_{x0} Q_{\infty \mathrm{d}} S_{\mathrm{ref}} z_{\mathrm{T}} - z_{\mathrm{G}} G \sin\theta_{\mathrm{d}}}{\mu_{\mathrm{L}} G \cos\theta_{\mathrm{d}}}, \tag{31}$$

where $Q_{\infty \mathrm{d}} = \dfrac{1}{2}\rho_{\mathrm{air}} V_{\mathrm{a0}}^2$ denote the dynamic pressure at steady state.

Setting the simulation parameters as $\mu_{\mathrm{L}} = 0.05$, $\rho_{\mathrm{air}} = 0.089\,\mathrm{kg/m^3}$, $k_2 = 2\sqrt{k_1}$, the initial position of slider $X_{\mathrm{L}}(0) = \bar{X}_{\mathrm{Ld}}|_{\theta_{\mathrm{d}}=0}$. The comparison of attitude control response and coupling effect of airship in different control gain coefficients k_1 is shown in Fig. 10.

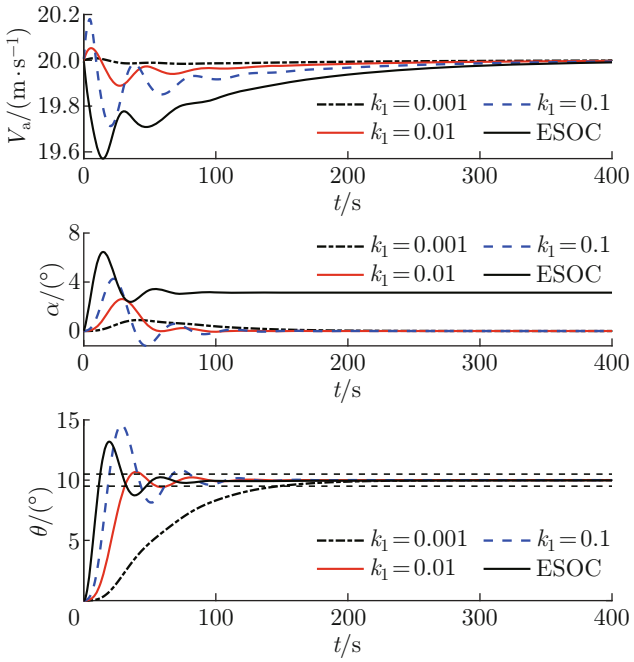

Fig. 10 Comparison of attitude control ability and coupling effect

In Fig. 10. Airspeed (V_{a}) and attack angle (α) are coupled differently under different k_1. While at the

final steady state moment, all the coupling effect will be disappeared, which indicates that the MMC method does not change the aerodynamic shape. In terms of attitude control response performance, if k_1 is too large, the pitching angle will be overshoot, while too small will deteriorate the control response capability. Thus, k_1 should be carried out by comprehensively considering the overshoot and adjustment time of attitude response. According to the simulation results, the attitude response has better dynamic performance by selecting $k_1 = 0.01$, which overshoot remains within 8%, the rise time $t_r \approx 32\,\mathrm{s}$, and the adjustment time $t_s(\Delta = 0.05) \approx 64\,\mathrm{s}$.

The black real curves in Fig. 10 are the attitude and velocity response curves when the elevator step open-loop control (ESOC) is adopted in attitude tracking. By comparison, the ESOC can quickly adjust the attitude, but also produces a coupling effect on the velocity of airship. However, the coupling effect on the attack angle cannot be eliminated at the steady-state time, which should be compensated by other control forces. This is the main difference between aerodynamic control surface and MMC mechanism in attitude control.

Figure 11 shows that although $\bar{X}_{\mathrm{Ld}}$ varies because the mass ratios is changed, and the attitude control response and the dynamic coupling effect of the slider are still keeping unchanged under the same slider controller parameters, which indicates that for the same attitude control target, the attitude control response characteristics of MMC are related to the slider controller parameters instead of the mass ratio of slider.

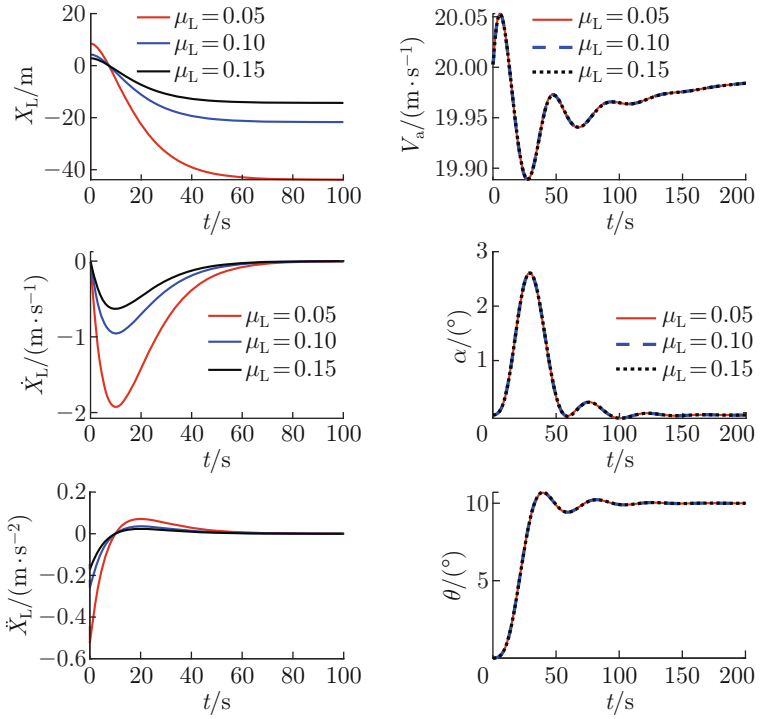

Fig. 11 Comparison of moving-mass attitude control response with different mass ratios

4.2.2 *Closed-Loop Attitude Control Response*

To further improve the dynamic performance of attitude control, the upper closed-loop controller can be designed by introducing tracking error feedbacks θ_{e} and $\dot{\theta}_{\mathrm{e}}$. The dynamic tracking position of slider is expressed as

$$\left.\begin{aligned} X_{\mathrm{Ld}} &= \bar{X}_{\mathrm{Ld}} + k_3\theta_{\mathrm{e}} + k_4\dot{\theta}_{\mathrm{e}} \\ \theta_{\mathrm{e}} &= \theta - \theta_{\mathrm{d}} \\ \dot{\theta}_{\mathrm{e}} &= q - \dot{\theta}_{\mathrm{d}} \end{aligned}\right\}, \tag{32}$$

where k_3, k_4 denote the control gain coefficients in the upper attitude controller. Figure 12 shows the attitude closed loop control response comparison.

From Fig. 12, the closed-loop control can effectively improve the stability and response speed of attitude control. Compared with open-loop control, the expected tracking value $\bar{X}_{\mathrm{Ld}}$ is no longer a constant value under the feedback of tracking error, and the control gain coefficient k_1 increases by 50 times, which causes the dynamic response performance of slider is significantly improved. The control gain coefficients k_3 and k_4 of the upper controller are the main parameters to adjust the dynamic performance index of attitude control. The larger k_3 is, the faster attitude response speed and the larger overshoot are. Meanwhile, the dynamic change range of $\bar{X}_{\mathrm{Ld}}$ is enlarged. k_4 is mainly used to reduce overshoot and overcome oscillation, but inhibits

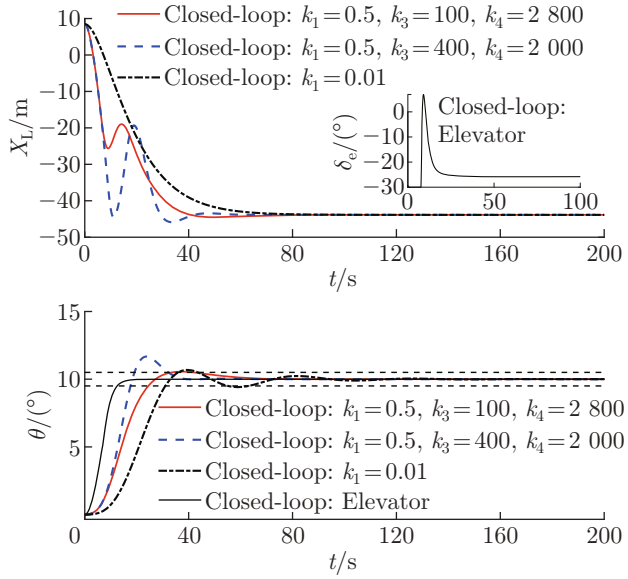

Fig. 12 Comparison of closed-loop control

the rise time of attitude response.

The black real curves in Fig. 12 represent the response curves of the closed-loop attitude control under the elevator. With the same error feedback control method by choosing $k_3 = 50$ and $k_4 = 150$, the first-order response time constant of the actuator is set as $\tau = 0.05\,\mathrm{s}$. Through comparatively analyzing the two types of control methods, the actuator δ_e has a shorter action time, and a better dynamic performance index of attitude control with faster response speed and non-overshoot. Therefore, if only considering the attitude control performance, the attitude control through aerodynamic control surface is more effective than the one by MMC in the operating capacity range.

4.2.3 *Dynamic Coupling Analysis*

The additional force and moment in the longitudinal plane produced by the dynamic response process of the slider can be obtained from Eq. (12):

$$\boldsymbol{P}_{\mathrm{mL}} = \begin{bmatrix} \Delta P_x \\ \Delta P_z \\ \Delta P_{\mathrm{m}} \end{bmatrix} = \begin{bmatrix} 1 & 0 & 0 & 0 & 0 & 0 \\ 0 & 0 & 1 & 0 & 0 & 0 \\ 0 & 0 & 0 & 0 & 1 & 0 \end{bmatrix} \boldsymbol{P}_{\mathrm{m}} = -m_{\mathrm{L}} \begin{bmatrix} \ddot{X}_{\mathrm{L}} \\ -2q\dot{X}_{\mathrm{L}} \\ b\ddot{X}_{\mathrm{L}} + 2qX_{\mathrm{L}}\dot{X}_{\mathrm{L}} \end{bmatrix}. \tag{33}$$

The additional acceleration effects on airship can be further analyzed qualitatively as:

$$\Delta \boldsymbol{a}_{\mathrm{L}} = \begin{bmatrix} \Delta \dot{u}_{\mathrm{m}} \\ \Delta \dot{w}_{\mathrm{m}} \\ \Delta \dot{m}_{\mathrm{m}} \end{bmatrix} = \boldsymbol{M}_{\mathrm{L}}^{-1} P_{\mathrm{mL}}. \tag{34}$$

Taking the two MMC methods corresponding to the red real curves in Fig. 10 (open-loop control) and Fig. 12 (closed-loop control) as examples, the changing processes of $\boldsymbol{P}_{\mathrm{mL}}$ are shown in Fig. 13, which shows that although the closed-loop control can improve the dynamic performance of attitude tracking, the stronger coupling effect on the airship and the more obvious oscillation of the slider will be taken. Comparing the influence on the axial force, it can be seen that $\Delta P_x \gg \Delta P_z$, and the additional acceleration effects caused by closed-loop control method are in the order of $\Delta \dot{u}_{\mathrm{m}} \in 10^{-1}\,\mathrm{m/s^2}$ and $\Delta \dot{w}_{\mathrm{m}} \in 10^{-3}\,\mathrm{m/s^2}$, respectively. The influence on pitching moment is proportional to ΔP_x, and the additional angular acceleration caused by closed-loop control method is in the order of $\Delta \dot{m}_{\mathrm{m}} \in 10^{-3}\,\mathrm{rad/s^2}$.

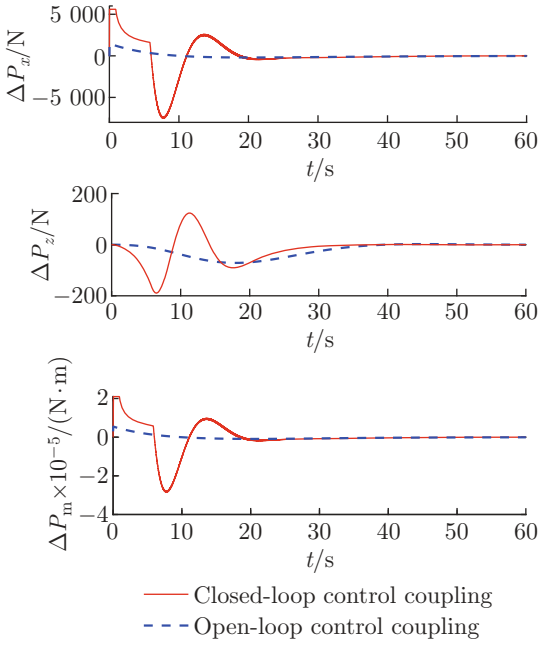

Fig. 13 Comparison of dynamic coupling

Therefore, if the dynamic performance index of attitude tracking under open-loop control method meets the design requirements, the steady-state tracking position $\bar{X}_{\mathrm{Ld}}$ can be directly used as the output of the upper attitude controller to minimize the complexity of controller design and the dynamic coupling effect on airship motion.

5 Conclusion

In this paper, a design method of moving-mass stratospheric airship based on constant total mass is presented, and the general dynamic equation is derived. For streamlined airships, the design scheme of MMC mechanism is proposed, and the attitude operation abilities of the two types of actuators under different airspeeds and mass ratios of slider are compared and

analyzed. A slider position tracking controller with critical damping is designed in the presence of input and state constraints. Combined with the dynamic response process of the slider, through the open-loop and closed-loop control simulation, the attitude control response ability and coupling characteristics of the two types of actuators for the airship motion are compared and analyzed. The main conclusions are as follows.

(1) The attitude operation ability of MMC method is only related to the mass ratio of the slider instead of airspeed.

(2) The slider position tracking system with critical damping characteristics can avoid the cut-off caused by response overshoot. For the same attitude control target, the attitude control response characteristics of MMC are related to the slider controller parameters instead of the mass ratio of slider.

(3) The closed-loop attitude control by MMC method has better dynamic performance index than that in open-loop control, but has a greater impact on the dynamic coupling of airship motion.

(4) In open-loop attitude control, the parameters of slider controller can directly affect the dynamic performance index of attitude tracking. If the index meets the design requirements, the complexity of controller design and the coupling effect of slider can be minimized by adopting the open-loop control method.

(5) The MMC method does not change the aerodynamic shape of the airship, and the airspeed and attack angle can converge to the initial state at the final steady state moment. If only considering the attitude control performance, the attitude control through aerodynamic control surface is more effective than the one by MMC in the operating capacity range.

In the future work, we will focus on the dynamic response characteristics and attitude control ability of moving-mass actuator, take the control efficiency and energy consumption as the optimization objectives, and carry out the research on the composite attitude control and allocation method based on MMC mechanism and aerodynamic control surface. At the same time, aimed at the problems of actuator failure, external disturbance and model inaccuracy, the fault-tolerant control should be studied.

References

[1] HOU Z X, YANG X X, QIAO K, et al. Stratospheric airship technology [M]. Beijing: Science Press, 2019 (in Chinese).

[2] ONDA M, MORIKAWA Y. High-altitude lighter-than-air powered platform [R]. Warrendale: SAE Technical Paper, 1991: 687-694.

[3] COLOZZA A, DOLCE J. Initial feasibility assessment of a high altitude long endurance airship: NASA CR-212724 [R]. Washington: NASA, 2003.

[4] CHU A, BLACKMORE M, OHOLENDT R, et al. A novel concept for stratospheric communications and surveillance: The StarLight [C]//*AIAA Balloon Systems Conference*. Williamsburg: AIAA, 2007: 2601.

[5] ZHENG W, YANG Y N, WU J. Survey of flight control for the stratosphere airship [J]. *Flight Dynamics*, 2013, **31**(3): 193-197 (in Chinese).

[6] REGAN F J, KAVETSKY R A. Add-on controller for ballistic reentry vehicles [J]. *IEEE Transactions on Automatic Control*, 1984, **12**(6): 869-880.

[7] DENG Y G, BAO Y P, LEI J W, et al. Research on composite control of new air vehicle [J]. *Acta Simulata Systematica Sinica*, 2005, **17**(7): 1531-1534 (in Chinese).

[8] GAO M W, SHAN X X. By changing position research of airship's center of gravity to control longitudinal motion [J]. *Chinese Quarterly of Mechanics*. 2006, **27**(4): 714-728 (in Chinese).

[9] SMITH I, LEE M K, FORTNEBERRY M, et al. HiSentinel80: flight of a high altitude airship [C]//*11th AIAA Aviation Technology, Integration, and Operations Conference*. Virginia Beach: AIAA, 2011: 6973.

[10] LEE M, SMITH I, ANDROULAKAKIS S. High-altitude LTA airship efforts at the US army SMDC/ARSTRAT [C]//*18th AIAA Lighter-Than-Air Systems Technology Conference*. Seattle: AIAA, 2009: 2852.

[11] ZHOU G, CHEN L, DONG Q. Modeling and analysis of moving-mass actuated stratospheric airship [J]. *High Technology Letters*, 2013, **19**(2): 145-149.

[12] WANG F, ZHOU J H, MIAO J G. Pitch handling characteristics of the stratospheric airship based on moving mass control [C]//*2016 35th Chinese Control Conference*. Chengdu: IEEE, 2016: 10915-10920.

[13] CHEN L, ZHOU G, YAN X J, et al. Composite control of stratospheric airships with moving masses [J]. *Journal of Aircraft*, 2012, **49**(3): 794-801.

[14] OUYANG J, QU W D, XI Y G. Stratospheric verifying airship modeling and analysis [J]. *Journal of Shanghai Jiao Tong University*, 2003, **37**(6): 956-960 (in Chinese).

[15] YANG Y N. Dynamics modeling and flight control for a stratospheric airship [D]. Changsha: National University of Defense Technology, 2013 (in Chinese).

[16] MIAO J G. Dynamics analysis & motion control of airship [D]. Beijing: University of Chinese Academy of Sciences (Space Science and Applications Research Center), 2008 (in Chinese).

[17] MUELLER J, PALUSZEK M, ZHAO Y. Development of an aerodynamic model and control law design for a high altitude airship [C]//*AIAA 3rd "Unmanned Unlimited" Technical Conference, Workshop and Exhibit*. Chicago: AIAA, 2004: 6479.

[18] OUYANG J. Research on modeling and control of unmanned airship [D]. Shanghai: Shanghai Jiaotong University, 2003 (in Chinese).

[19] SCHMITENDORF W E, BARMISH B R. Null controllability of linear systems with constrained controls [J]. *SIAM Journal on Control and Optimization*, 1980, **18**(4): 327-345.